Assembling responsive microgels at responsive lipid membranes

Meina Wang[a,1], Adriana M. Mihut[a,1], Ellen Rieloff[a], Aleksandra P. Dabkowska[a], Linda K. Månsson[a], Jasper N. Immink[a], Emma Sparr[a], and Jérôme J. Crassous[a,b]

[a]Physical Chemistry, Department of Chemistry, Lund University, SE-221 00 Lund, Sweden; and [b]Institute of Physical Chemistry, RWTH Aachen University, 52074 Aachen, Germany

Edited by Michael L. Klein, Institute of Computational Molecular Science, Temple University, Philadelphia, PA, and approved January 31, 2019 (received for review May 4, 2018)

Directed colloidal self-assembly at fluid interfaces can have a large impact in the fields of nanotechnology, materials, and biomedical sciences. The ability to control interfacial self-assembly relies on the fine interplay between bulk and surface interactions. Here, we investigate the interfacial assembly of thermoresponsive microgels and lipogels at the surface of giant unilamellar vesicles (GUVs) consisting of phospholipids bilayers with different compositions. By altering the properties of the lipid membrane and the microgel particles, it is possible to control the adsorption/desorption processes as well as the organization and dynamics of the colloids at the vesicle surface. No translocation of the microgels and lipogels through the membrane was observed for any of the membrane compositions and temperatures investigated. The lipid membranes with fluid chains provide highly dynamic interfaces that can host and mediate long-range ordering into 2D hexagonal crystals. This is in clear contrast to the conditions when the membranes are composed of lipids with solid chains, where there is no crystalline arrangement, and most of the particles desorb from the membrane. Likewise, we show that in segregated membranes, the soft microgel colloids form closely packed 2D crystals on the fluid bilayer domains, while hardly any particles adhere to the more solid bilayer domains. These findings thus present an approach for selective and controlled colloidal assembly at lipid membranes, opening routes toward the development of tunable soft materials.

microgel | lipid | vesicle | colloid | membrane

Colloidal self-assembly at fluid interfaces represents an efficient bottom-up nanofabrication approach to create materials with well-defined and tunable properties. Interfacial colloidal assembly has many applications in material, biomedical, and food sciences, including photonic materials, sensors, and formulations in food and drug delivery systems (1–6). One major challenge in the development of these fields lies in the ability to control the colloidal self-assembly to build up well-defined structures such as colloidal crystals with long-range order (4–13), which relies on basic understanding of how the chemical and physical properties of the colloid systems influence the interparticle interactions (6, 11, 14–17). The colloidal building blocks are diverse and range, in terms of internal elasticity, from hard spheres, such as polystyrene and silica particles (7, 8, 12, 13), to soft colloids—for example, as polymeric microgels (18–26). For the case of polymeric microgels, the particle softness can be altered within the very same colloidal system by varying the external conditions in terms of temperature, pH, or ionic strength (26–29).

The fluid interface can provide a versatile template that can be used to generate highly ordered and tunable 2D structures (23–25), which recently found some application for nanolithography (25). The potential of mediating the assembly of responsive colloids on fluid interfaces has been extensively exploited to create tunable crystalline colloidal arrays at the interfaces of emulsion oil droplets (30–35). Recently, we demonstrated that this approach could be extended to nanometer-thin lipid bilayer membranes (36). These findings open up possibilities to use responsive colloids for constructing functional nanostructured biomolecular surfaces. However, these previous studies were focused on systems of simple oil or fluid membrane systems with properties that remain almost unaffected for the range of conditions investigated. In the present work, we introduce an additional tool for controlling interfacial self-assembly in the use of a responsive interface composed of a lipid membrane that alters its structure and dynamics with changes in the external conditions.

Inspired by applications of nanocarriers in drug-delivery systems, and by the potential risks involved with the increased exposure to nanomaterials, numerous theoretical and experimental studies have focused on elucidating conditions for adsorption and translocation of nanoparticles and microparticles across lipid membranes within biological systems (37–46). These systems are generally highly complex, and the particle–membrane interactions will depend on many parameters of the system, including nanoparticle size and shape (44, 47–54) and surface chemistry (51, 55–61), as well as the charge, composition, and curvature of the membrane (45). In many cases, it remains arduous to single out the key parameters for preferential adsorption or translocation of particles across a lipid membrane or biological interface. Even though most biological systems are soft and deformable,

Significance

Soft microgel-based colloids consisting of a responsive polymer network offer an ideal platform for exploring the interactions between nanomaterials and artificial model membranes. Here, we report a modality to pattern and assemble responsive colloids as microgels or lipogels—i.e., microgels associated with small lipid vesicles—to desired locations on phospholipid giant unilamellar vesicles. The tunable properties of the microgels—for example, softness, deformability, hydrophobicity, and thermosensitivity—are used to manipulate and guide the adsorption and assembly behavior. This study reveals that phospholipid bilayers are versatile molecular templates for defined and highly ordered interfacial assemblies, 2D colloidal crystals, and selective patterning as imposed by the fluidity of the membrane.

Author contributions: M.W., A.M.M., A.P.D., E.S., and J.J.C. designed research; M.W., A.M.M., E.R., A.P.D., L.K.M., and J.N.I. performed research; M.W. and J.J.C. analyzed data; M.W., A.M.M., E.S., and J.J.C. wrote the paper; and L.K.M. and J.N.I. performed synthesis and characterization of the microgels.

The authors declare no conflict of interest.

This article is a PNAS Direct Submission.

[1]To whom correspondence may be addressed. Email: crassous@pc.rwth-aachen.de or adrianacrassous@gmail.com.

This article contains supporting information online at www.pnas.org/lookup/suppl/doi:10.1073/pnas.1807790116/-/DCSupplemental.

Published online March 1, 2019.

the role of particle softness for the particle–membrane interactions is still not fully understood (36, 61). Here, the combination of responsive colloids and membranes can offer possibilities for investigating interactions in these systems.

In the present study, we use a model system where we are able to alter the properties of both particles and membrane within the very same sample by varying the temperature between ∼17 and 40 °C. We use systems composed of thermoresponsive microgel and lipogel particles, the latter being obtained by the coating of microgels with lipid bilayers (62). These particles are added to responsive phospholipid membranes of giant unilamellar vesicles (GUVs). Both types of particles were shown to adsorb to the fluid membranes without any signs of translocation. We further explore how interfacial particle structure and dynamics can be controlled by altering the properties of the lipid membrane and the colloid particles, and we demonstrate that the single lipid bilayers can be used as scaffolds to build 2D colloidal crystals. The present study can thus provide insights into how colloids interact with lipid membranes, and it demonstrates a templating approach that can have applications in the development of novel responsive bioinspired materials.

Results

We monitored adsorption and rearrangement of microgel particles at the lipid bilayer scaffold of GUVs using confocal laser-scanning microscopy (CLSM). The lipid bilayers were composed of zwitterionic phospholipids [phosphatidylcholine (PC) and phosphatidylethanolamine (PE)] with varying chain length to enable studies of solid–fluid phase transitions, domain formation, and lipid headgroup size (64). The N-isopropylacrylamide (PNIPAM) microgel particles were either directly added or assembled beforehand with PC lipids to form lipogel particles. The particles are thermoresponsive, and the volume-phase transition temperature of the bare particles (T_{VPT}) was determined to 32 °C by dynamic light-scattering (DLS) measurement (*SI Appendix*, Fig. S1*A*). The particles were slightly cationic, as confirmed by electrophoretic mobility measurements (*SI Appendix*, Fig. S1*B*). The particle charge is due to the presence of amidine end groups arising from the initiator during the particle synthesis (for details on particle synthesis and characterization, see *SI Appendix* and refs. 34 and 36). Below T_{VPT}, the particles are swollen and hydrophilic, whereas above T_{VPT}, they are collapsed and more hydrophobic (34, 36). The GUVs were prepared by using the electroformation method in a fluidic channel with indium tinoxide (ITO)-coated glass slides (Fig. 1 *A* and *B*). The experimental setup and protocols were here developed to allow for in situ observations of the particle adsorption and reorganization at the membrane surface. This setup offers clear advantages compared with previous protocols, where the particles were present during the GUV formation process (36), as it offers the possibility to directly resolve adsorption or translocation phenomena. Due to the narrow channels, it is possible to image single vesicles over several hours. In addition, with this setup, one can avoid artifacts that might arise under conditions where vesicles are filled with solution of higher density than water (sucrose or glucose), which is a common approach in many studies in the literature with the goal to make the vesicles sediment and arrest (65).

Particle Adsorption on Fluid Lipid Bilayers: Effect of Particle Conformation. The adsorption of fluorescently labeled PNIPAM microgel particles [fluorescein *O*-methacrylate (FMA); green] on GUVs composed of 1,2-dioleoyl-*sn*-glycero-3-phosphatidylcholine (DOPC) (Fig. 1*C*) and a small amount (0.5 mol%) fluorescent lipid analogue (Rhod-PE; red) was investigated at different temperatures. The phospholipids form a bilayer structure with fluid acyl chains (L_α phase) for the entire temperature range investigated. The PNIPAM microgel particles, on the other hand, respond to changes in temperature, going from swollen hydrophilic to collapsed more hydrophobic structures at temperatures around T_{VPT}. The cartoons in Fig. 2*A* illustrate the state of particles and lipids at each temperature. The adsorption process of microgel particles was studied for DOPC GUVs at 20 °C. Particle adsorption was observed within a few minutes after the addition of the dispersed particles to the flow cell. The adsorbed particles diffuse in the plane of the bilayer interface to form 2D crystalline domains with a hexagonal arrangement (Movie S1). After ∼20–30 min, the whole surface is covered by the crystalline lattice of particles. The arrangement of 2D colloidal crystals was maintained even after rinsing with water to remove an excess of unadsorbed particles (Fig. 2 *B* and *E*), and there was no measurable desorption of particles at this temperature. The 2D hexagonal packing of the particles was confirmed from the analysis of the pair correlation function, $g(r)$, and the average center-to-center distance, r_{max}, was measured to ∼1.0 μm (*SI Appendix*, Fig. S2). This value is slightly larger than the particle hydrodynamic D_H in the bulk, as derived from DLS to 0.90 μm (34) (*SI Appendix*, Fig. S1*A*). The same interfacial particle arrangement was confirmed for DOPC vesicles with no added Rh-PE dye, confirming that the observed effect was not due to specific interactions between the particles and the fluorescent lipid analogue (*SI Appendix*, Fig. S3*A*). A similar experiment was also performed for lipid vesicles

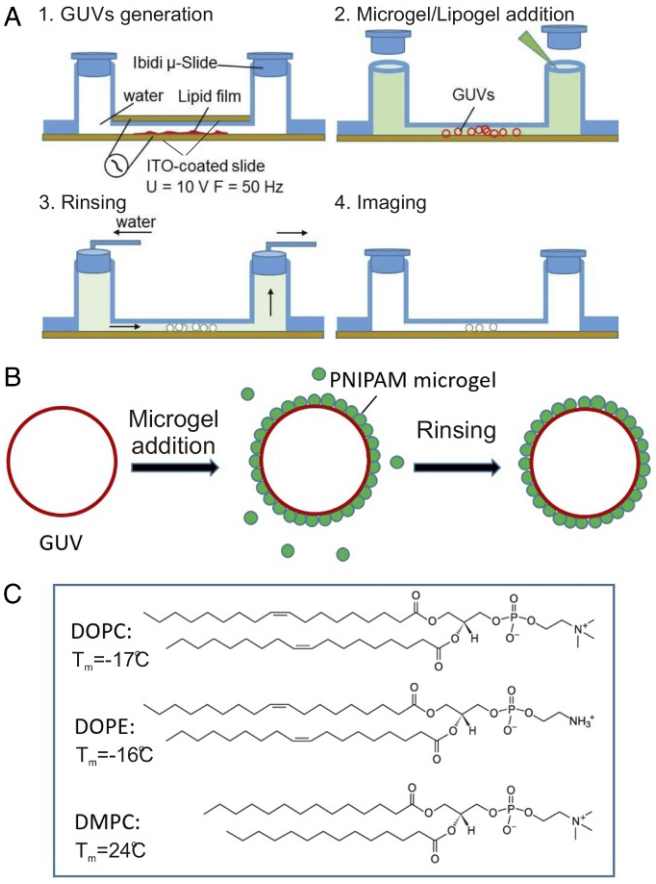

Fig. 1. (*A* and *B*) Schematic representation of the experimental protocol. GUVs were produced from a hydrated lipid film after application of an alternating electric field (63) in a millifluidic cell. Microgels or lipogels are then added. After adsorption, the excess free particles are washed away by gently rinsing with water. (*C*) Molecular structures of different lipids used to form GUVs in the present study together with the chain melting temperatures of these lipids dispersed in excess water.

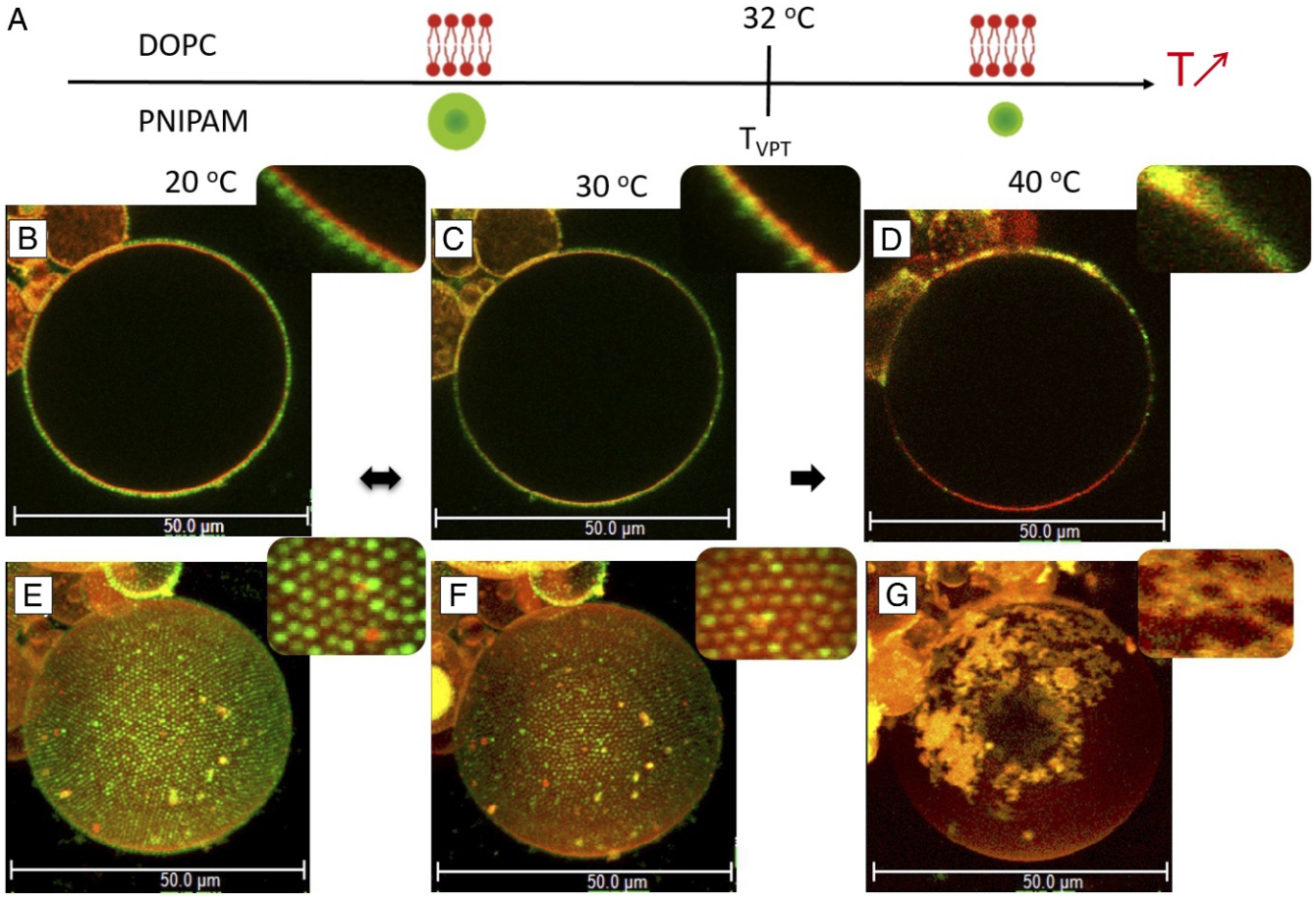

Fig. 2. (*A*) Schematic representation of DOPC membrane and a thermoresponsive PNIPAM particle as a function of temperature. Below T_{VPT}, microgel particles are swollen, soft, and hydrophilic, whereas above T_{VPT}, they are collapsed, harder, and more hydrophobic. The lipid DOPC membrane is fluid over the whole temperature-interval investigated. (*B–G*) Fluorescence confocal micrographs showing a giant DOPC vesicle decorated with PNIPAM particles at 20 °C (*B* and *E*), 30 °C (*C* and *F*), and 40 °C (*D* and *G*). *B–D*, *Insets* reveal close-up views of lateral cross-sections showing the GUV–microgels contact line. (*E–G*) The 3D intensity projections of confocal *z*-stacks [51.67 (*x*) × 51.67 (*y*) × 68.58 (*z*) μm^3]. *E–G*, *Insets* show close-up views of particle organizations at the surface of the GUV.

with 20 mol% 1,2-dioleoyl-*sn*-glycero-3-phosphoethanolamine (DOPE) added to the DOPC membrane. DOPE has a smaller headgroup compared with DOPC, and it can therefore promote nonlamellar structures (66). It was concluded that this change of the physical and chemical properties of the lipid membrane has no detectable effect on the particle adsorption and 2D crystallization (*SI Appendix*, Fig. S4).

After the microgel adsorption at the DOPC GUVs was complete at 20 °C, the very same sample was investigated over a range of temperatures. Fig. 2 shows 2D and 3D confocal images of one single vesicle with adsorbed particles at 20, 30, and 40 °C. As described above, the adsorbed particles arranged into 2D colloidal crystals with hexagonal packing at the GUV at 20 °C, covering the whole vesicle surface. When the temperature was increased to 30 °C, which is close to T_{VPT} of the free particles, the adsorbed particles slightly collapsed, and they appeared partially embedded in the lipid membrane (Fig. 2 *C* and *F*). The average distance between the centers of two neighboring particles was determined to 0.82 μm (*SI Appendix*, Fig. S2), which is comparable to D_H = 0.82 μm measured in bulk at the same temperature (*SI Appendix*, Fig. S2). When the temperature was increased further to 40 °C, we observed that most of the collapsed particles desorbed from the vesicle interface. Here, the remaining adsorbed particles form aggregates at the membrane, losing their well-defined 2D organization (Fig. 2 *D* and *G*). Colocalization of red and green dyes in the aggregates further indicates that the adsorbed colloidal clusters also contain lipids.

In the next step, the very same sample was cooled down from 40 °C to 20 °C (*SI Appendix*, Fig. S3*B*). From this experiment, we confirmed that the remaining adsorbed particles formed islands with no further signs of particle aggregation. Furthermore, the adsorbed particles did not seem to be lipid-loaded, and they were packed in a partial monolayer. Interestingly, the size and shape of the GUVs determined from the 3D CLSM projections (Fig. 2 *E–G*) remained almost constant over the whole temperature cycle, which indicates that the desorption process does not lead to substantial extraction of lipids from the membrane. Finally, we conclude that the particles do not translocate across the lipid bilayer for any of the conditions investigated.

Particle Adsorption on Fluid/Solid Lipid Bilayers: Effect of Lipid-Phase Transitions. The lipid phase can be switched between bilayer structures with fluid and solid acyl chains by varying, for example, acyl chain composition or temperature (64, 67). The fluid (L_α) bilayer phase is characterized by high lateral diffusion and low order parameter of the acyl chains, while the gel-phase bilayer phase is characterized by low lateral diffusion and highly ordered acyl chains (64, 67). Due to the differences in lipid packing between these two bilayer phases, the effective area per lipid

headgroup is increased by ∼30% when going from the gel to the fluid bilayer, which directly implies increased exposure of the hydrophobic interior of the bilayer to the surrounding aqueous solution (68).

We investigated the influence of the solid–fluid lipid-phase transition on the adsorption and lateral organization of microgels using 1,2-dimyristoyl-*sn*-glycero-3-phosphocholine (DMPC) (Fig. 1*C*) as a model system. In excess solution conditions, the chain-melting transition temperature of DMPC, T_M, is ∼24 °C. In this experiment, the microgel particles were first adsorbed to the DMPC GUVs at 30°C, which is well above the lipid-melting transition. The excess nonadsorbed particles were then washed away, and the very same sample was further studied at different temperatures. After each temperature change, the samples were left to equilibrate for 2 h, which was considered enough time for a single bilayer to reach the equilibrium bilayer phase. Representative micrographs recorded at different temperatures are shown in Fig. 3*A*: 30 °C (above T_M), 24 °C (close to T_M), and 17 °C (below T_M). At 30 °C, the particles adsorb at the fluid bilayer to form a 2D crystalline monolayer, whereas the excess of free particles tend to aggregate into clusters in the bulk solution (Fig. 3 *B* and *E*) as the colloids start to collapse at this temperature (36). When the temperature was changed to T_M (24 °C), the particle organization in a 2D crystalline configuration at the fluid bilayer was maintained (Fig. 3 *C* and *F*). The microgel-decorated DMPC vesicles closely resemble those formed in the system composed of DOPC and microgel particles at 20 °C (Fig. 2), which is not surprising because the lipids contain the same headgroup and form similar bilayer structure. When the temperature was further decreased to 17 °C, the lipid chains became ordered and the bilayer became solid. Under these conditions, most of the particles desorbed from the membrane, and the remaining adsorbed particles were randomly distributed at the solid DMPC bilayer (Fig. 3 *D* and *G*). There were no signs of 2D crystal formation below the DMPC chain-melting temperature. On the other hand, when the system containing DOPC vesicles and microgel particles was cooled to the same temperature (20 °C), the 2D crystalline organization was maintained. We therefore conclude that the phase transition in the lipid bilayer directly perturbs the 2D hexagonal crystalline ordering of the colloids and that it lowers the affinity of the particles for the bilayer interface. When the temperature was again raised above T_m from 20 °C to 30 °C, the particles remaining at the DMPC GUVs surface regained their mobility, as shown in Movie S2.

To further investigate the role of membrane fluidity, we prepared GUVs composed of DMPC/DOPC (75/25 molar ratio). This lipid mixture formed coexisting solid–fluid bilayer domains over a range of temperatures, as inferred from the phase diagram and the DSC data (Fig. 4*A* and *SI Appendix*, Fig. S5). This model lipid system makes it possible to distinguish preferential adsorption of the microgel particles to certain domains in membranes that contain more than one bilayer phase (Fig. 4 *B–D*).

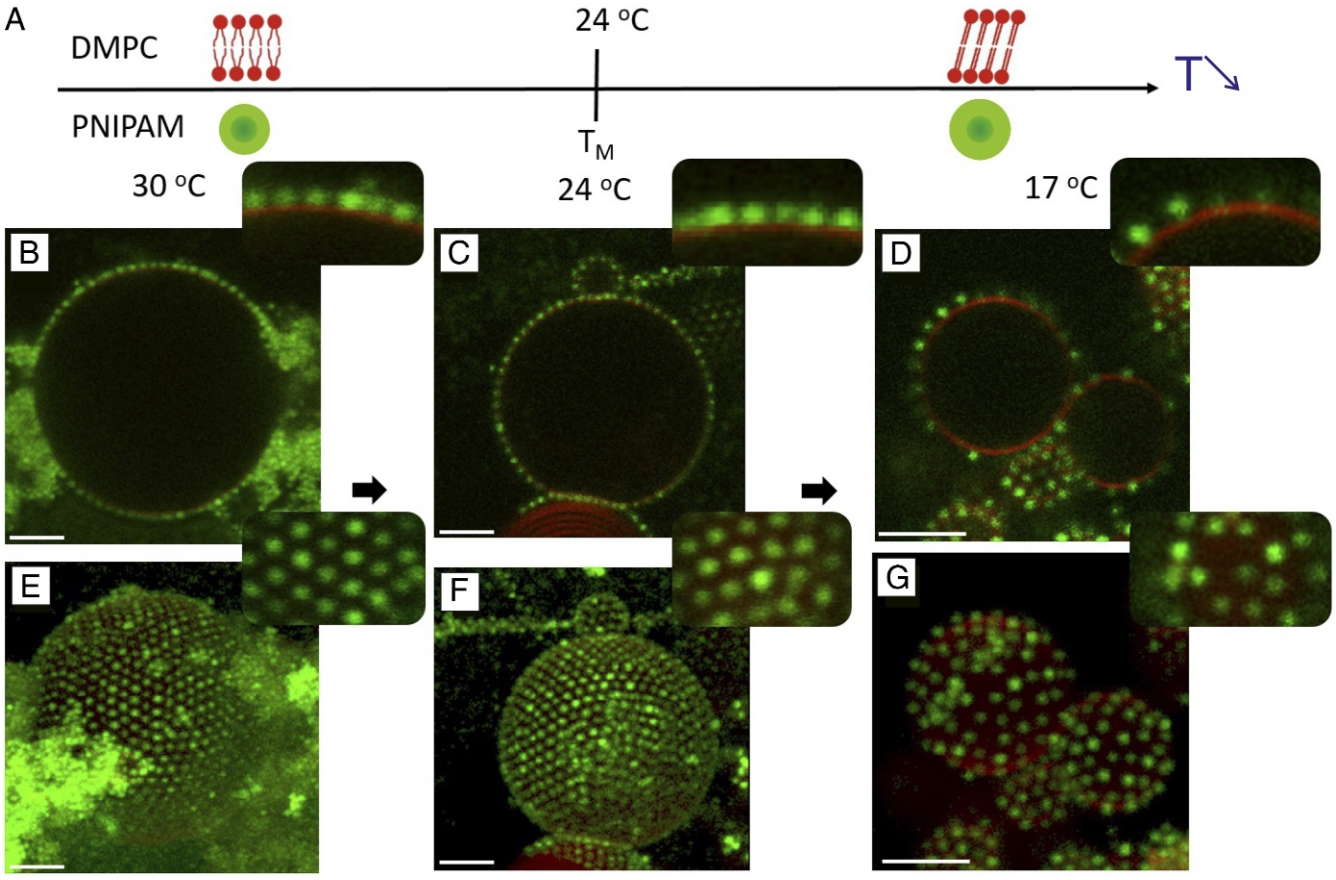

Fig. 3. (*A*) Schematic representation of DMPC membrane and a thermoresponsive PNIPAM particle as a function of temperature. Below the melting temperature, T_M, the DMPC forms gel-phase bilayers with solid chains, and above T_M, DMPC forms bilayers with fluid chains. In the investigated temperature range, the microgel particles are swollen and hydrophilic. (*B–G*) Fluorescence confocal micrographs showing DMPC GUVs decorated with PNIPAM particles at 30 °C (*B* and *E*), 24 °C (*C* and *F*), and 17 °C (*D* and *G*). *B–D*, *Insets* reveal close-up views of lateral cross-sections of GUV-microgels contact lines. (*E–G*) The 3D intensity projections of confocal *z*-stacks, supported by close-up views of particle organizations at the surface of the GUVs shown as *Insets*. (Scale bars: 5 μm.)

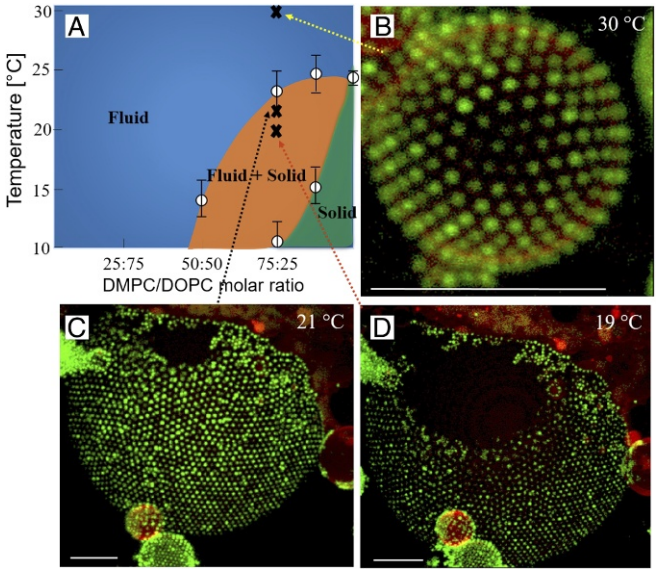

Fig. 4. (*A*) Phase diagram of DOPC/DMPC lipids based on differential scanning calorimetry (DSC) data. (*B*) Fluorescence confocal micrographs of GUVs consisting of a mixture of DOPC/DMPC (75/25). At the highest temperature, 30 °C, when the whole bilayer forms a single fluid bilayer, the surface is homogeneously decorated with microgel particles. (*C* and *D*) When temperature is decreased, the lipid membrane separates into domains consisting of fluid and solid bilayer phases. The red fluorescent lipid analogue is only present in the fluid domains, and the solid domains appear black in the images. Images were taken at 21 °C (*C*) and 19 °C (*D*) showing the growth of the solid domains at lower temperature. It is clearly demonstrated that the microgel particles show strong preference of the fluid domains where it adsorbs to form 2D hexagonal crystals. Only very few particles were detected in the solid domains. (Scale bars: 10 μm.)

At 30 °C, the lipid membrane forms a single fluid bilayer phase. The microgel particles were then added to the GUV sample at this temperature and start to adsorb into a monolayer with a hexagonal packing (Fig. 4*B*), similar to that observed for GUVs composed of DOPC and DMPC alone (Figs. 2 *C* and *F* and 3 *B* and *E*). The same sample was then cooled down to given temperature corresponding to conditions where we expect two-phase coexistence. At 21 °C (Fig. 4*C*), segregated domains composed of either fluid bilayer or gel-phase bilayer structure were formed. The fluorescent lipid analogue was excluded from the more solid domains, which thus appear dark in the confocal images. It is a clear conclusion that the microgel particles are almost exclusively found at the fluid bilayer domains, again forming 2D colloid crystals with hexagonal arrangement. At an even lower temperature (19 °C), the gel-phase domains cover larger areas of the vesicle surface (Fig. 4*D*). No further changes in the proportion of solid and fluid domains were observed after the 2-h equilibration. As the interparticle distance at the fluid domain remained the same from 21 °C to 19 °C, we conclude that the microgel particles were desorbing from the solid domains rather than packing more closely. The particle preference for the fluid bilayer phase will likely lead to the stabilization of these domains and broadening of the two-phase region. We here conclude that, for the present system and conditions, these effects are relatively small, as the overall lipid phase behavior with a solid–fluid phase transition in this temperature regime remains.

Lipogel Adsorption on Fluid Lipid Bilayers. Following the detailed characterization of microgel adsorption to phospholipid bilayers, we investigated the adsorption and lateral arrangement in a more complex colloidal particle system using lipid-loaded microgels, usually referred to as lipogels (62). The lipogels were prepared by incubating PNIPAM particles with small unilamellar DOPC vesicles (SUVs) (Fig. 5*A*). For the given lipid/particle ratio (mass ratio microgel/lipid 1/2; here named lipid-rich lipogels), the lipids entirely covered the microgel particles, as the green fluorescence of copolymerized FMA from the particle appeared completely surrounded by the red Rhod-PE fluorescent lipid analogue (Fig. 5*B*).

Fig. 5*C* shows a series of 2D and 3D confocal images of lipid-rich lipogels adsorbed at the lipid bilayer of the DOPC GUV at 20 °C. In this experiment, the scaffold bilayer in the GUV is labeled with the green fluorescent probe, NBD-PE, and the lipid associated with the lipogel contains the red lipid analogue Rh-PE. We conclude that the lipogels adsorb to the lipid bilayer in a similar manner as the bare microgel particles, forming 2D crystals with a hexagonal lattice. The analysis of the pair correlation function, $g(r)$, of the lipogels in the 2D crystals configuration revealed an average center-to-center distance of ∼0.88 μm, which is smaller compared with the situation when bare microgels were adsorbed at the DOPC bilayer at the same temperature. In other words, the lipogels appear more compressed or more closely packed in the 2D crystals compared with the bare PNIPAM particles. Another striking observation in Fig. 5*C* is that the lipids associated with the microgel in the lipogel particles do not appear to fuse with the scaffold membrane in the GUV within the time frame of the experiment, as is apparent from the absence of red fluorescence signal in the GUV bilayer. Indeed, the confocal images in Fig. 5*C* infer that the lipogel-associated lipids are depleted from the interfacial region between the particle and the scaffold membrane in the GUV, only covering the parts of the particles that face the aqueous solution.

The lipogel adsorption experiments on unlabeled GUVs were repeated with lipogels prepared with five times less lipid (mass

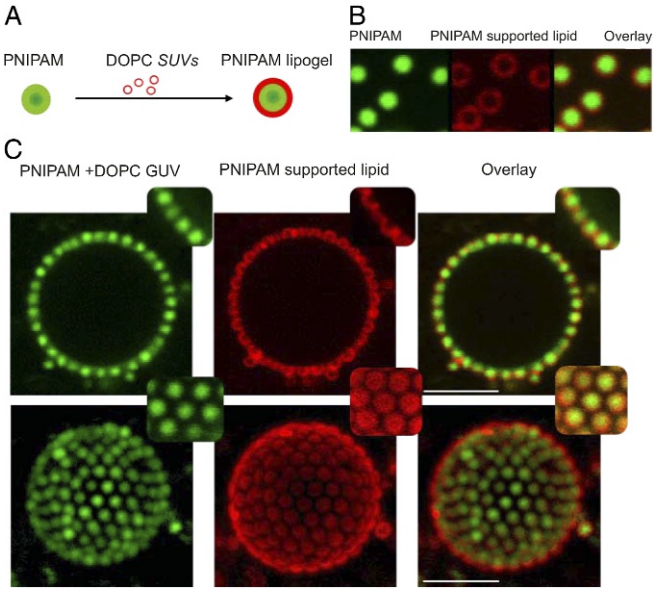

Fig. 5. (*A*) Schematic illustration of lipogel preparation from PNIPAM particles and DOPC SUVs. (*B*) Fluorescence micrographs of lipid-rich lipogels adsorbed at a GUV, from left to right, showing green fluorescence of copolymerized FMA present in PNIPAM, red fluorescence of Rhod-PE present in DOPC lipid, and the overlay of the two channels. (*C*) The 2D and 3D micrographs of NBD-PE–labeled DOPC GUVs decorated with lipid-rich lipogels. From left to right: green fluorescence of copolymerized FMA in PNIPAM microgels and NBD-PE in GUVs, red fluorescence of Rhod-PE present in coated lipid, and the overlay of the two channels. *Insets* show close-up views of lateral cross-sections and at the top of the GUVs. Temperature: 20 °C. (Scale bars: 5 μm.)

ratio microgel/lipid 1/10; here named lipid-poor lipogels). The individual lipogels adsorbed at the glass coverslip exhibited some incomplete lipid coverage of the microgel (*SI Appendix*, Fig. S6*A*). Under these conditions, the lipogels adsorbed to the GUVs and rearranged in a more disordered fashion as compared with the lipid-rich lipogel particles (*SI Appendix*, Fig. S6*B*).

Discussion

The formation of the particle–bilayer contact lines implies deformations of both the particles and the membrane. When the adhesion is sufficient, the particles will wrap at the interface to a certain extent. We here treat the case of fluid bilayers formed by one lipid species in giant vesicles (radius $\sim$10 μm). In relation to the lipid molecules, the bilayer is considered as planar, and we therefore do not consider effects of membrane asymmetry, as previously treated for smaller vesicles (45). Following the description proposed by Dietrich et al. (69) for the adhesion of latex spheres to GUVs and further developed in other studies (38, 70, 71), we first assume a nondeformable spherical colloid with a radius R_P adsorbed and partially wrapped at the surface of a deformable lipid bilayer, as depicted in *SI Appendix*, Fig. S7*A*. The degree of wrapping, z, is characterized by the angle, α, defined by the contact line and the center of the particles following:

$$z = 1 - cos(\alpha). \quad [1]$$

The area of the lipid covered by the particles is expressed through

$$A_{ad} = 2\pi R_P^2 z, \quad [2]$$

and the adhesion energy follows as

$$E_{adh} = -\omega A_{ad}. \quad [3]$$

The related bending energy is given by:

$$E_{bend,ad} = \frac{2\kappa A_{ad}}{R_p^2}, \quad [4]$$

where κ is the bending rigidity of the membrane. By adsorbing the particles, the work against the lateral tension σ is proportional to the excess area pulled toward the wrapping site, corresponding to $\pi R_P^2 z^2$ at the origin of the tension energy

$$E_{ten,ad} = \pi R_P^2 z^2 \sigma. \quad [5]$$

The last term to describe the total energy of the system is related to the energy of the bare membrane with no adsorbed particles, E_{free}, which is less straightforward to estimate, as discussed in ref. 71. The total energy of the system is then given by the sum of the different terms following:

$$\begin{aligned} E_{tot} &= E_{ad} + E_{bend} + E_{ten} + E_{free} \\ &= 4\pi z\kappa + \pi R_P^2 (z^2\sigma - 2\omega z) + E_{free}. \end{aligned} \quad [6]$$

We consider that E_{free} is negligible compared with the other contributions to the total energy, which is expected for a low surface coverage and low wrapping. The system is at equilibrium when $-E_{ad} \approx E_{bend} + E_{ten}$. The minimization of Eq. **6** with respect to z indicates that the particles do not adhere to the bilayer when $\omega < \omega_c = 2\kappa/R_P^2$, where ω_c is the critical adhesion energy (38, 70, 71). Partial wrapping is then expected for larger ω-values, and a full wrapping ($z = 2$) is expected for $\omega \geq \omega_c + \sigma$. Thus, determining α and therefore the degree of wrapping, z leads to an estimate of the adhesion energy per surface, ω, given by:

$$\omega \approx \frac{2\kappa}{R_P^2} + \frac{z\sigma}{2}. \quad [7]$$

α can be roughly estimated experimentally from the CLSM micrographs by looking to the degree of indentation of the particles. This is achieved by monitoring the particles adsorbed at the surface of the GUVs. The position of the bilayer at contact is determined from its maximum fluorescence as well as the center of the adsorbed particles (*SI Appendix*, Fig. S7*A*). Assuming that the particles are nondeformable, and that their size is rendered by their hydrodynamic radius, α was determined to $37 \pm 5^\circ$ from statistical analysis over 50 configurations. However, the relatively small size of the particles and their fast diffusion at the interface limit the accuracy of such measurements (*SI Appendix*). We can now estimate ω for a typical DOPC bilayer assuming $\kappa \approx 20 k_B T$ (60) and $R_P = 450$ nm. The calculations were performed for different σ-values (*SI Appendix*, Fig. S7*B*). $\sigma = 2 \times 10^{-5}$ N/m was considered in the case of a tense bilayer, the value of which is in the range of cellular membrane tension (72). $\sigma \approx 1 \times 10^{-6}$ N/m corresponds to the critical value reported in a recent study on DOPC GUVs for tense vesicles (60) and for other lipid bilayers (73). The dashed line corresponds to $\omega_c = 2\kappa/R_p^2$. The corresponding adhesion energy is thus estimated between $\sim 8 \times 10^{-7}$ and 2.8×10^{-6} J/m^2. Such ω-values are in the order of what was found for DOPC GUVs and micrometric polystyrene particles coated with avidin presenting a similar size as our microgels ($R_P \approx 490$ nm, $\omega \approx 6.8 \times 10^{-7}$ J/m^2). These particles were found to wrap on floppy membranes ($\sigma < 10$ nN/m) and, conversely, only to adsorb on tense vesicles, and no complete wrapping could be observed for $\sigma > 1$ μN/m (60). In the present study, the GUVs do not present any apparent shape fluctuations; we will therefore in the following consider them as tense, corresponding to $\sigma \geq 10^{-6}$ N/m. Increasing the temperature, R_p decreases from 450 nm at 20 °C to 280 nm at 40 °C. Assuming that ω is constant, the size decrease is accompanied by a decrease of the particle wrapping (Eq. **7**). This effect is illustrated for $\omega = 8 \times 10^{-7}$ J/m^2 and $\omega = 30 \times 10^{-7}$ J/m^2 and for different σ-values (*SI Appendix*, Fig. S8). As such, the desorption above T_{VPT} can be partially understood from the deswelling of the particles. Following this approach for nondeformable collapsed microgels ($R_p = 280$ nm at 40 °C), the particles are expected to desorb when $\omega \lesssim \omega_c = 2.2 \times 10^{-6}$ J/m^2.

In the discussion above, we assume nondeformable particles. However, microgels are soft colloids which are characterized by their relatively low elastic modulus, E, usually ranging from 10 to 100 kPa (74, 75). We can get an order of magnitude of the extent of their deformation, assuming their adsorption at a planar interface by using the Derjaguin model for adhesive contact (76, 77). It is important to note that the Derjaguin model of adhesive contact here only provides an order of magnitude for the deformation. More accurate and detailed models may lead to complex contact configurations (77) that need to be considered together with the mechanical properties and deformation of the membrane. To our knowledge, such a theoretical model is still missing and needs to be implemented in the future to properly describe the wrapping of soft particles at lipid membrane. Within this model, the microgels are considered as Hertzian bodies, which was shown to be a good approximation for their interactions in bulk in the limit of small deformations (28, 78). A schematic representation is provided in *SI Appendix*, Fig. S9*A*. Assuming that the Hertz relation between contact radius and penetration is preserved, the contact radius, a, can be estimated as (76):

$$a \approx \left(\frac{\pi\omega R_p^2}{E^\star}\right)^{\frac{1}{3}}, \quad [8]$$

where $E^\star = E/(1-\nu^2)$ and ν is the Poisson ratio. The penetration corresponding to the microgel flattening at the surface is given by the relation:

$$\delta = \frac{a^2}{R_p}. \quad [9]$$

For swollen microgel particles, $\nu \approx 0.25$, whereas in the collapsed state, $\nu \approx 0.5$ (79, 80). In addition, the volume transition is accompanied by an increase of E by approximately an order of magnitude (74). *SI Appendix*, Fig. S9 *B* and *C* provides estimates of a and δ as a function of R_p for swollen and collapsed particles, with $E = 10$ and 100 kPa considering either a strong adhesion ($\omega = 3 \times 10^{-6}$ J/m^2) or weak adhesion ($\omega = 8 \times 10^{-7}$ J/m^2). In the limit of a strong adhesion for a soft microgel, the deformation, $\delta/R_P \approx 1.6\%$, confirming the absence of a strong deformation at the interface. It decreases to $\sim$0.4% in the collapsed state. Under the same conditions, $a \approx 56$ nm for a swollen soft microgel and $\sim a \approx 18$ nm for a harder collapsed microgel. Therefore, the decrease of size and softness are expected to lead to a significant reduction of the contact area and local deformation, facilitating the desorption of the microgels at high temperatures.

When the particles are adsorbed to the lipid membrane, they reorganize in the plane of the membrane to form a highly ordered and closely packed monolayer structure (Movie S1). Such reorganization implies high lateral diffusion of particles in the plane of the bilayer, which is only fulfilled for the fluid bilayer phases (64). From this, we infer that a fluid membrane can host and mediate long-range ordering of closed packed colloids in contrast to the more solid gel-phase membrane. This is analogous to previous observations of biomacromolecules, such as RNA and streptavidin, forming closely packed and ordered single layers at fluid lipid bilayers (81–84). The organization of particles in the plane of the bilayer can be analyzed with respect to the interparticle distances. For fluid lipid bilayers at 20 °C (Fig. 2 and *SI Appendix*, Fig. S4), we observed that the particles adsorb and diffuse at the lipid interface to ultimately organize into crystals with a lattice parameter $\sim$10% larger than their hydrodynamic diameter. Interestingly, this value strongly differs from that measured for the same type of microgel particles at polydimethylsiloxane oil droplets in microgel-stabilized emulsion, where the particles arrange into 2D crystals with lower lattice parameter corresponding and an average interparticle distance of $\sim$0.72 μm, which is 20% smaller than the hydrodynamic diameter of the particles (*SI Appendix*, Fig. S10) (34). The DOPC bilayer in the GUVs is assumed to present a low bending rigidity and a high lateral tension for the present conditions with no added salt (60). Under these conditions, the tension energy is high and can overcome the bending energy for large particles and high lateral tension. In our case, it typically corresponds to $\sigma > 8 \times 10^{-6}$ J/m^2 for $R_p = 450$ nm and $\alpha = 37°$. Hereby, the partial wrapping of the particles generates an additional stress related to the displacement of the lipids that can be released by bending the bilayer in the opposite direction (*SI Appendix*, Fig. S11). As long as the particle is only partially wrapped and the contact angle, α (defined by the contact and the center of the particles) is $<2\alpha \leq \pi$, we expect the wrapping of the particles to be at the origin of an additional repulsion proportional to $z^2 R_P^2 \sigma$. For more details on the model, refer to *SI Appendix* and *SI Appendix*, Fig. S11. The simple model outlined above illustrates the fundamental difference between the particle adsorption at lipid bilayers and microgel-stabilized emulsion droplets. At emulsion droplets, microgels usually experience attractive capillary interactions (30, 31, 85), whereas for adsorption at the bilayer, the partial wrapping of the particles may be at the origin of repulsive interparticle interactions. From the relative interparticle center-to-center distance, the model provides an estimate of $\alpha \approx 33°$, which is consistent with the experimental observations of $\alpha \approx 37°$ for the DOPC fluid bilayers at 20 °C. When the temperature was increased to 30 °C, the particle-size decrease may be reflected by a diminution of z and the release of the additional tension, leading to a more disordered organization and to a shorter r_{max} relative to the hydrodynamic diameter.

Microgels and lipogel particles were observed to adsorb to fluid phospholipid bilayers, and, in the adsorbed layer, they exhibit high lateral mobility, allowing for efficient reorganization and formation of large 2D crystalline arrays. In the DMPC lipid system, the decrease in temperature below the fluid-to-solid phase transition leads to partial desorption of the particles, as well as arrested dynamics of the remaining adsorbed particles. The particle dynamics at the bilayer is shown to be reversible with respect to the lipid-phase behavior, as particles adsorbed at the gel-phase bilayer can be "reactivated" and regain their mobility by increasing the temperature above lipid chain melting temperature. The close correlation between the particle dynamics and the state of the membrane indicates that swollen microgels closely interact with the lipid bilayer at the molecular level through their protruding polymer chains.

We can here rule out electrostatic interactions as the dominant source of attraction, as adsorption of swollen cationic microgel particles to the zwitterionic DOPC, DMPC, and DOPC/DOPE is observed for all cases where the bilayer is in a fluid state and also in the absence of the anionic Rh-PE lipid dye, while it is not seen in cases of solid bilayers, even though these are composed of the same lipids. The driving force for the PNIPAM microgel adsorption to the fluid lipid bilayer is likely related to the relatively high solubility of the protruding polymeric dangling chains in the fluid hydrophobic layer of the bilayer. In a gel-state bilayer, on the other hand, the acyl chains are frozen, and the lipids are more densely packed. The hydrophobic interior of the bilayer is thus less exposed to the aqueous surrounding. Furthermore, the solid lipid acyl chains are a less good solvent to the penetrating polymer chains from the microgel. Together, this can explain the low adsorption of microgel particles to the gel-phase bilayer domains.

The coassembled microgel–lipid particles, so-called lipogels, adsorb to the lipid bilayer to form 2D crystalline arrays, similar to the bare microgels. However, the lattice parameter for the crystalline monolayer of lipogels is clearly smaller as compared with the microgel 2D lattice, which is probably related to the shrinking of the microgels that are associated with lipids. The size of the lipogel could not be determined in bulk solution, as the association with lipids leads to reduced colloidal stability in the system. A slow coagulation of the lipogels was observed in bulk for the lipid-rich lipogels in Fig. 5. A twofold increase in the lipid in respect to the lipid-rich lipogels composition was shown to result in a fast coagulation process. It was further noted that the lipogel particles are easily redispersed by vortexing, pointing to the weak attractive component in the interparticle interactions. We thus envision the coassembly of lipids and microgels into lipogels with given composition as a means to control the attraction between the colloids. This can be compared with the situation when one adds a small amount of immiscible liquids, creating bridging through capillary interactions (86, 87).

For all lipid–particle ratios investigated, the weak interparticle attraction explains that the lipogels have enough mobility to densely pack and organize at the bilayer interface. However, the incomplete coverage of the microgels results in the segregation of the adsorbed lipid into an outer layer (bridging mode) (Fig. 5*B*) or to local connections at lower lipid composition (pendling mode) (*SI Appendix*, Fig. S6*B*). In a control experiment, we added labeled SUVs to unlabeled GUVs. The absence of fluorescence of the GUVs confirmed that there was no detectable fusion of SUVs with the GUV bilayer within the time frame of the experiments. Together, these experiments illustrate the preferential affinity of the lipids for the microgels and the possibility to control the particle and lipid distribution at the adsorbed layer. The formation of a lipid layer covering the

outer surface of the adsorbed microgel monolayer may offer a route to create tunable supported lipid membranes on microgel cushions as an alternative to surface-tethered polymer cushions (88, 89).

Conclusion

We have demonstrated that the interactions between thermoresponsive microgel particles and GUV lipid bilayers can be tuned and controlled with the temperature. At low temperature ($T \leq 30$ °C), the soft, swollen microgel colloids show preferential adsorption to fluid lipid membranes compared with solid membranes and were found to organize into 2D crystals with a hexagonal order at the fluid membrane. When temperature or lipid composition was changed to induce solid bilayer structures, particles desorbed from the solid regions. At 40 °C, i.e., above the volume phase transition of the microgels, the microgel particles undergo a change of their conformation from swollen to collapsed. The 2D crystalline arrangement at the fluid membrane observed at lower temperatures is then lost, and most of the particles desorb from the GUVs, which we explain by the decrease of their size and softness. Furthermore, we have shown that microgels loaded with lipids, so-called lipogels, can also densely pack at fluid GUVs, offering the possibility to control both the microgel and lipid organization as a function of the lipogel composition. We believe that the possibility to manipulate and dynamically guide microgel self-assembly at fluid–lipid interfaces will pave the way toward the development of novel soft functional biomaterials and inspire future investigations on the interactions between soft colloids and membranes.

Materials and Methods

Materials. DMPC (M_W 677.94, $C_{36}H_{72}NO_8P$), DOPE (M_W, 744.034, $C_{41}H_{78}NO_8P$), DOPC (M_W 786.113, $C_{44}H_84NO_8P$); 1,2-dioleoyl-*sn*-glycero-3-phosphoethanolamine-*N*-(lissamine rhodamine B sulfonyl) (ammonium salt; Liss Rhod-PE, M_W 1,301.75, $C_{68}H_{109}N_4O_{14}PS_2$), and 1,2-dioleoyl-*sn*-glycero-3-phosphoethanolamine-*N*-(7-nitro-2-1,3-benzoxadiazol-4-yl; ammonium salt) ($C_{47}H_82N_5O_11P$; NBD-PE; ∼98 % purity) were purchased from Avanti Polar Lipids. Chloroform (analytical grade, ≥ 99.8%) was purchased from Sigma-Aldrich. Methanol (analytical grade, ≥ 99.9%) was purchased from Merck. *N*-isopropylacrylamide, *N*, *N*′-methylenebisacrylamide, 2,2′-azobis(2-methylpropionamidine) dihydrochloride, and FMA were all purchased from Sigma and used as received. Milli-Q water was used in all the experiments. The PNIPAM microgel particles were synthesized by using 5 mol% cross-linker and FMA as labeled by precipitation polymerization as described in former studies (34, 36) and in *SI Appendix*.

Preparation of Lipid Stock Solutions. The stock solutions of DOPC and DMPC with 0.5 mol% Liss Rhod-PE were mixed to achieve 1:3 molar ratio. The stock solutions of DOPC and DOPE with Liss Rhod-PE were mixed to achieve 4:1 molar ratio. For systems containing more than one lipid species, the lipids were mixed to reach the given molar ratio in the chloroform/methanol solution. The lipid solutions were stored in the freezer.

Preparation of GUVs in Milli-Q Water. GUVs were formed on ITO-coated microscope coverslips by using the electroformation method. The ITO-coated coverslips were cleaned with chloroform and dried under nitrogen. A 10-μL lipid solution with 0.5 mol% Liss Rhod-PE was deposited onto the conductive side of the ITO-coated glass and allowed to dry for at least 12 h. After totally drying, the lipid-coated side of the ITO-coated glass was mounted to a self-adhesive underside of a microchannel (Ibidi Sticky-Slide VI 0.4; height, 0.4 mm; length of channel, 17 mm; width of channel, 3.8 mm). The second ITO-coated glass was attached to the top side of the microchannel with the conductive side toward the sample. Conductive tape was then used to connect the conductive side of the two ITO-coated glasses to the electrode from the frequency generator. An ac field of 10 V operating at a frequency of 50 Hz was applied for >2 h to generate the GUVs.

Adsorption of Microgel Particles at Lipid Bilayer. After producing the GUVs, the microgel particle dispersion was added into the fluidic channel and imaged by confocal microscopy. The GUV/particle sample was left still until the adsorption process was completed. Afterward, the excess particles in the fluidic channel were gently washed away.

PNIPAM Lipogel Preparation. SUVs were first prepared by using a probe sonicator (Vibra-Cell, Sonics Materials Inc.). A total of 2.1 mg of DOPC with 0.5 mol% Rhod-PE was weighted in and dissolved in chloroform. Chloroform was evaporated under nitrogen flow and was totally dried in a vacuum chamber for 12 h. The resultant dry lipid film was rehydrated in 2 mL of Millipore water, vortexed, and left to stand for 30 min. Lipid dispersions were sonicated to clarity (10 s on, 10 s off for 15 min), while taking care not to overheat the sample. The resultant aqueous solution (1.05 mg/mL, 0.5 mL) was then added to PNIPAM microgel dispersion (1 mg/mL, 1 mL) stepwise over 10 min to fabricate what we refer to as lipid-rich lipogels. Lipid-poor lipogels were prepared following the same procedure with a more dilute SUVs dispersion (0.21 mg/mL, 0.5 mL) added to microgel dispersion (1 mg/mL, 1 mL).

CLSM. A Leica SP5 confocal laser-scanning microscope operated in the inverted mode (D6000I) was used to monitor fluorescent GUV/particle samples at different temperatures. The confocal laser-scanning microscope was mounted in a thermostated enclosure, which enabled temperature control with an accuracy of 0.2 °C. Samples were cooled down with a cooling rate ∼20–30 °C/h and equilibrated for 2 h at each temperature before examination. The red fluorescence of the membrane marker (Liss Rhod-PE) and the green fluorescence of fluorescein (FMA) were excited by using a 543-nm HeNe and a 488-nm Ar ion laser. For each GUV/particle sample, two sets of images were required: 2D image (*xy* slice) and 3D projection reconstructed from confocal *z*-stack images. Only decorated vesicles, which were not in direct contact with the ITO substrate, were imaged.

ACKNOWLEDGMENTS. This work was supported by Knut and Alice Wallenberg Foundation Project Grant KAW 2014.0052. J.J.C. was supported by the Deutsche Forschungsgemeinschaft within SFB 985 Functional Microgels and Microgel Systems.

1. Meseguer F (2005) Colloidal crystals as photonic crystals. *Colloids Surf A* 270: 1–7.
2. Velikov KP, Velev OD (2006) *Novel Materials Derived from Particles Assembled on Liquid Surfaces*, eds. Binks BP, Horozov TS (Cambridge Univ Press, Cambridge, UK), pp 225–297.
3. Dickinson E (2006) *Interfacial Particles in Food Emulsions and Foams*, eds. Binks BP, Horozov TS (Cambridge Univ Press, Cambridge, UK), pp 298–327.
4. Böker A, He J, Emrick T, Russell TP (2007) Self-assembly of nanoparticles at interfaces. *Soft Matter* 3:1231–1248.
5. Grzelczak M, Vermant J, Furst EM, Liz-Marzán LM (2010) Directed self-assembly of nanoparticles. *ACS Nano* 4:3591–3605.
6. McGorty R, Fung J, Kaz D, Manoharan VN (2010) Colloidal self-assembly at an interface. *Mater Today* 13:34–42.
7. Pieranski P (1980) Two-dimensional interfacial colloidal crystals. *Phys Rev Lett* 45: 569–572.
8. Horozov TS, Aveyard R, Clint JH, Binks BP (2003) Order-disorder transition in monolayers of modified monodisperse silica particles at the octane-water interface. *Langmuir* 19:2822–2829.
9. Roldughin VI (2004) Self-assembly of nanoparticles at interfaces. *Russ Chem Rev* 73:115–145.
10. Binder WH (2005) Supramolecular assembly of nanoparticles at liquid–liquid interfaces. *Angew Chem Int Edition* 44:5172–5175.
11. Bergström L (2006) *Structure and Formation of Particle Monolayers at Liquid Interfaces*, eds. Binks BP, Horozov TS (Cambridge Univ Press, Cambridge, UK), pp 77–107.
12. Ray MA, et al. (2009) Submicrometer surface patterning using interfacial colloidal particle self-assembly. *Langmuir* 25:7265–7270.
13. Isa L, et al. (2010) Particle lithography from colloidal self-assembly at liquid-liquid interfaces. *ACS Nano* 4:5665–5670.
14. Binks BP, Horozov TS (2006) *Colloidal Particles at Liquid Interfaces: An Introduction*, eds. Binks BP, Horozov TS (Cambridge Univ Press, Cambridge, UK), pp 1–74.
15. Fernández-Toledano JC, Moncho-Jordá A, Martínez-López F, Hidalgo-Álvarez R (2006) Theory for interactions between particles in monolayers, eds. Binks BP, Horozov TS (Cambridge Univ Press, Cambridge, UK), pp 108–151.
16. Bresme F, Oettel M (2007) Nanoparticles at fluid interfaces. *J Phys Condens Matter* 19:413101–413133.
17. Park BJ, Lee D, Furst EM (2015) Chapter 2 interactions and conformations of particles at fluid-fluid interfaces. *Particle-Stabilized Emulsions and Colloids: Formation and Applications* (The Royal Society of Chemistry, London), pp 8–44.
18. Zhang J, Pelton R (1999) Poly(*N*-isopropylacrylamide) microgels at the air-water interface. *Langmuir* 15:8032–8036.

19. Brugger B, Vermant J, Richtering W (2010) Interfacial layers of stimuli-responsive poly-(*N*-isopropylacrylamide-co-methacrylicacid) (PNIPAM-co-MAA) microgels characterized by interfacial rheology and compression isotherms. *Phys Chem Chem Phys* 12:14573–14578.
20. Geisel K, Isa L, Richtering W (2012) Unraveling the 3D localization and deformation of responsive microgels at oil/water interfaces: A step forward in understanding soft emulsion stabilizers. *Langmuir* 28:15770–15776.
21. Geisel K, Rudov AA, Potemkin II, Richtering W (2015) Hollow and core–shell microgels at oil–water interfaces: Spreading of soft particles reduces the compressibility of the monolayer. *Langmuir* 31:13145–13154.
22. Wellert S, Richter M, Hellweg T, von Klitzing R, Hertle Y (2015) Responsive microgels at surfaces and interfaces. *Z Phys Chem* 229:1225–1250.
23. Picard C, et al. (2017) Organization of microgels at the air–water interface under compression: Role of electrostatics and cross-linking density. *Langmuir* 33:7968–7981.
24. Rauh A, et al. (2017) Compression of hard core-soft shell nanoparticles at liquid-liquid interfaces: Influence of the shell thickness. *Soft Matter* 13(1):158–169.
25. Scheidegger L, et al. (2017) Compression and deposition of microgel monolayers from fluid interfaces: Particle size effects on interface microstructure and nanolithography. *Phys Chem Chem Phys* 19:8671–8680.
26. Plamper FA, Richtering W (2017) Functional microgels and microgel systems. *Acc Chem Res* 50:131–140.
27. Lyon LA, Fernandez-Nieves A (2012) The polymer/colloid duality of microgel suspensions. *Annu Rev Phys Chem* 63:25–43.
28. Paloli D, Mohanty PS, Crassous JJ, Zaccarelli E, Schurtenberger P (2013) Fluid–solid transitions in soft-repulsive colloids. *Soft Matter* 9:3000–3004.
29. Yunker PJ, et al. (2014) Physics in ordered and disordered colloidal matter composed of poly(*N*-isopropylacrylamide) microgel particles. *Rep Prog Phys* 77:056601.
30. Destribats M, et al. (2011) Soft microgels as pickering emulsion stabilisers: Role of particle deformability. *Soft Matter* 7:7689–7698.
31. Destribats M, et al. (2013) Pickering emulsions stabilized by soft microgels: Influence of the emulsification process on particle interfacial organization and emulsion properties. *Langmuir* 29:12367–12374.
32. Richtering W (2012) Responsive emulsions stabilized by stimuli-sensitive microgels: Emulsions with special non-pickering properties. *Langmuir* 28:17218–17229.
33. Li Z, Ngai T (2015) Emulsions stabilized by soft microgel particles. *Particle-Stabilized Emulsions and Colloids: Formation and Applications* (The Royal Society of Chemistry, London), pp 93–128.
34. Månsson LK, Immink JN, Mihut AM, Schurtenberger P, Crassous JJ (2015) A new route towards colloidal molecules with externally tunable interaction sites. *Faraday Discuss* 181:49–69.
35. hin Kwok M, Ngai T (2016) A confocal microscopy study of micron-sized poly(*N*-isopropylacrylamide) microgel particles at the oil–water interface and anisotopic flattening of highly swollen microgel. *J Colloid Interf Sci* 461:409–418.
36. Mihut AM, Dabkowska AP, Crassous JJ, Schurtenberger P, Nylander T (2013) Tunable adsorption of soft colloids on model biomembranes. *ACS Nano* 7:10752–10763.
37. Mukherjee S, Ghosh RN, Maxfield FR (1997) Endocytocis. *Physiol Rev* 77:759–803.
38. Lipowsky R, Döbereiner HG (1998) Vesicles in contact with nanoparticles and colloids. *Europhys Lett* 43:219–225.
39. Conner SD, Schmid SS (2003) Regulated portals of entry into the cell. *Nature* 422: 37–44.
40. Rejman J, Oberle V, Zuhorn IS, Hoekstra D (2004) Size-dependent internalization of particles via the pathways of clathrin- and caveolae-mediated endocytosis. *Biochem J* 377:159–169.
41. Rothen-Rutishauser BM, Schürch S, Haenni B, Kapp N, Gehr P (2006) Interaction of fine particles and nanoparticles with red blood cells visualized with advanced microscopic techniques. *Environ Sci Technol* 40:4353–4359.
42. Leroueil PR, et al. (2006) Nanoparticle interaction with biological membranes: Does nanotechnology present a janus face? *Acc Chem Res* 40:335–342.
43. Nel AE, et al. (2009) Understanding biophysicochemical interactions at the nano–bio interface. *Nat Mater* 8:543–557.
44. Liu Y, Tan J, Thomas A, Ou-Yang D, Muzykantov VR (2012) The shape of things to come: Importance of design in nanotechnology for drug delivery. *Ther Deliv* 3: 181–194.
45. Agudo-Canalejo J, Lipowsky R (2015) Critical particle sizes for the engulfment of nanoparticles by membranes and vesicles with bilayer asymmetry. *ACS Nano* 9:3704–3720.
46. Meng X, Li X (2018) Size limit and energy analysis of nanoparticles during wrapping process by membrane. *Nanomaterials* 8:899.
47. Decuzzi P, Ferrari M (2006) The adhesive strength of non-spherical particles mediated by specific interactions. *Biomaterials* 27:5307–5314.
48. Yang K, Ma YQ (2010) Computer simulation of the translocation of nanoparticles with different shapes across a lipid bilayer. *Nat Nanotechnol* 5:579–583.
49. Tao L, et al. (2011) Shape-specific polymeric nanomedicine: Emerging opportunities and challenges. *Exp Biol Med* 236:20–29.
50. Shah S, Liu Y, Hu W, Gao J (2011) Modeling particle shape-dependent dynamics in nanomedicine. *J Nanosci* 11:919–928.
51. Vácha R, Martinez-Veracoechea FJ, Frenkel D (2011) Receptor-mediated endocytosis of nanoparticles of various shapes. *Nano Lett* 11:5391–5395.
52. Bahrami AH, et al. (2014) Wrapping of nanoparticles by membranes. *Adv Colloid Interf Sci* 208:214–224.
53. Dasgupta S, Auth T, Gompper G (2014) Shape and orientation matter for the cellular uptake of nonspherical particles. *Nano Lett* 14:687–693.
54. Dasgupta S, Auth T, Gompper G (2017) Nano- and microparticles at fluid and biological interfaces. *J Phys Condens Matter* 29:373003.
55. Verma A, et al. (2008) Surface-structure-regulated cell-membrane penetration by monolayer-protected nanoparticles. *Nat Mater* 7:588–595.
56. Wang B, Zhang L, Bae SC, Granick S (2008) Nanoparticle-induced surface reconstruction of phospholipid membranes. *Proc Natl Acad Sci* 105:18171–18175.
57. Schulz M, Olubummo A, Binder WH (2012) Beyond the lipid-bilayer: Interaction of polymers and nanoparticles with membranes. *Soft Matter* 8:4849–4864.
58. da Rocha EL, Caramori GF, Rambo CR (2013) Nanoparticle translocation through a lipid bilayer tuned by surface chemistry. *Phys Chem Phys* 15:2282–2290.
59. Barnoud J, Rossi G, Monticelli L (2014) Lipid membranes as solvents for carbon nanoparticles. *Phys Rev Lett* 112:068102.
60. van der Wel C, et al. (2016) Lipid membrane-mediated attraction between curvature inducing objects. *Sci Rep* 6:32825.
61. Yi X, Gao H (2016) Incorporation of soft particles into lipid vesicles: Effects of particle size and elasticity. *Langmuir* 32:13252–13260.
62. Saleem Q, Liu B, Gradinaru CC, Macdonald PM (2011) Lipogels: Single-lipid-bilayer-enclosed hydrogel spheres. *Biomacromolecules* 12:2364–2374.
63. Angelova MI, Dimitrov D (1986) Liposome electroformation. *Faraday Discuss Chem Soc* 81:303–311.
64. Cevc G (2007) *Phospholipids Handbook* (Taylor & Francis, Abingdon, UK), 2nd Ed.
65. Morales-Penningston NF, et al. (2010) {GUV} preparation and imaging: Minimizing artifacts. *Biochim Biophys Acta Biomembr* 1798:1324–1332.
66. Shalaev EY, Steponkus PL (1999) Phase diagram of 1,2-dioleoylphosphatidylethanolamine (dope):water system at subzero temperatures and at low water contents. *Biochim Biophys Acta Biomembr*. 1419:229–247.
67. Evans D, Wennerström H (1999) The colloidal domain: Where physics, chemistry, biology, and technology meet, *Advances in Interfacial Engineering* (Wiley, New York).
68. Mihailescu M, et al. (2011) Acyl-chain methyl distributions of liquid-ordered and -disordered membranes. *Biophys J* 100:1455–1462.
69. Dietrich C, Angelova M, Pouligny B (1997) Adhesion of latex spheres to giant phospholipid vesicles: Static and dynamics. *J Phys II France* 7:1651–1682.
70. Deserno M, Bickel T (2003) Wrapping of a spherical colloid by a fluid membrane. *Europhys Lett* 62:767–774.
71. Deserno M (2004) Elastic deformation of a fluid membrane upon colloid binding. *Phys Rev E* 69:031903.
72. Morris CE, Homann U (2001) Cell surface area regulation and membrane tension. *J Membr Biol* 179:79–102.
73. Evans E (1992) Equilibrium "wetting" of surface by membrane-covered vesicles. *Adv Colloid Interf Sci* 39:103–128.
74. Hashmi SM, Dufresne ER (2009) Mechanical properties of individual microgel particles through the deswelling transition. *Soft Matter* 5:3682–3688.
75. Monteillet H, et al. (2014) Ultrastrong anchoring yet barrier-free adsorption of composite microgels at liquid interfaces. *Adv Mater Inter* 1:1300121.
76. Derjaguin BV (1934) Untersuchungen über die reibung und adhäsion. *Kolloid Z* 69:155–164.
77. Barthel E (2008) Adhesive elastic contacts—JKR and more. *J Phys D* 41:163001.
78. Rovigatti L, Gnan N, Ninarello A, Zaccarelli E (2018) On the validity of the Hertzian model: The case of soft colloids. ArXiv:1808.04769. Preprint, posted August 14, 2018.
79. Hirotsu S (1991) Softening of bulk modulus and negative Poisson's ratio near the volume phase transition of polymer gels. *J Chem Phys* 94:3949–3957.
80. Boon N, Schurtenberger P (2017) Swelling of micro-hydrogels with a crosslinker gradient. *Phys Chem Chem Phys* 19:23740–23746.
81. Brisson A, Olofsson A, Ringler P, Schmutz M, Stoylova S (1994) Two-dimensional crystallization of proteins on planar lipid films and structure determination by electron crystallography. *Biol Cel* 80:221–228.
82. Reviakine I, Brisson A (2001) Streptavidin 2D crystals on supported phospholipid bilayers: Toward constructing anchored phospholipid bilayers. *Langmuir* 17: 8293–8299.
83. Horton MR, Reich C, Gast AP, Rädler JO, Nickel B (2007) Structure and dynamics of crystalline protein layers bound to supported lipid bilayers. *Langmuir* 23:6263.
84. Dabkowska AP, et al. (2015) Assembly of RNA nanostructures on supported lipid bilayers. *Nanoscale* 7:583–596.
85. Huang S, et al. (2016) Microgels at the water-oil interface: In situ observations of structural aging and two-dimensional magnetic bead microrheology. *Langmuir* 32:712–722.
86. Knoos E, Willenbacher N (2011) Capillary forces in suspension rheology. *Science* 331:897–900.
87. Bossler F, Knoos E (2016) Structure of particle networks in capillary suspensions with wetting and nonwetting fluids. *Langmuir* 32:1489–1501.
88. Wagner ML, Tamm LK (2000) Tethered polymer-supported planar lipid bilayers for reconstitution of integral membrane proteins: Silane-polyethyleneglycol-lipid as a cushion and covalent linker. *Biophys J* 79:1400–1414.
89. Smith HL, et al. (2009) Model lipid membranes on a tunable polymer cushion. *Phys Rev Lett* 102:228102.